Infrared Absorption Spectroscopy of the $^{14}N_2^+$ Meinel System 2-1 Band

By

Bogdan Negru

Thesis

for the

Degree of Bachelor of Science

in

Chemistry

College of Liberal Arts and Sciences

University of Illinois

Urbana-Champaign, Illinois

2007

Table of Contents:

Acknowledgements:

I would like to thank Professor Ben McCall for his guidance and continued support. I would like to thank Dr. Susanna Widicus Weaver for her work with the spectrometer and for her advice. I would like to thank Michael Wiczer for calibrating the spectrum and Josh DiGangi for building the discharge cell. I would like to thank Brian Tom for his help with the spectrometer. I would like to thank the McCall group for their help and encouragement. I would like to thank Christopher G. Tarsitano for supplying the fitting routine used in the analysis. I would like to thank my friends and family for the priceless emotional support they have given me. Most of all, I would like to thank my parents for their sacrifice and for making this possible.

Infrared absorption spectroscopy of the $^{14}N_2^+$ Meinel system 2-1 band

I. Introduction:

The $A^2\prod_u$-$X^2\sum_{g^+}$ system of N_2^+ has been extensively studied since the early stages of the twentieth century. The first mention was made by Childs[1] in 1932 proposing the existence of the $A^2\prod_u$ excited state, which was confirmed by Meinel eighteen years later while observing auroral emissions in the near-infrared[2]. Despite the intimidating challenge posed by molecular ion spectroscopy, the laboratory characterization of N_2^+ has a long and diverse history, beginning in 1951 with a publication from Dalby and Douglas[3], and continuing in present day experiments. The $A^2\prod_u$-$X^2\sum_{g^+}$ system of N_2^+ became known as the Meinel system; and the model Hamiltonian used in this work was published in a very thorough paper by Miller et al.[4] in 1984.

The study of similar molecular ions that can be performed with our new spectrometer is of great significance for chemistry, physics, and astrochemistry. The N_2^+ cation is especially important in atmospheric phenomena, as it is a major constituent of the ionosphere[5] and of a large variety of electrical discharges[6]. N_2^+ is a popular target for high resolution spectroscopy, so it was a very appropriate choice as the first test for our continuous-wave cavity ring down spectrometer. The accuracy of the available N_2^+ data in the 9000 to 14500 cm^{-1} range[7] is quite low, and the (2,1) band has never been observed before. This study offers the first laboratory observation of the N_2^+ (2,1) band, and it involves a high-resolution continuous wave cavity ringdown spectrometer. A fit was obtained for the assigned transitions in this band and the improved values of the previously predicted molecular constants will be shown in this work.

II. Experimental Design:

We have developed a high resolution gas-phase spectrometer that can be used for the study of a wide range of molecular species with astrochemical or atmospheric interest, and began our work with the study of N_2^+. The high resolution direct absorption technique used by this spectrometer, sketched in Figure 1, is continuous wave Cavity Ringdown Spectroscopy (cw-CRDS). The chief benefit of CRDS is that kilometer sized path lengths are achieved, resulting in very high sensitivities. Ringdown spectroscopy is a versatile technique that can be combined with different molecular sources, such as a supersonic expansion or a cold cathode ion source, to allow for studies of scientific interest to be performed.

The laser source used for CRDS can be continuous wave or it can be pulsed. The benefits for using a continuous wave laser source, like the one used in this experiment, are that the spatial and spectral purities are significantly higher[8]. The laser is coupled to one cavity mode when an integral or half integral number of wavelengths fit inside the cavity, so the light waves constructively interfere and an increase in intensity takes place. Once the intensity threshold required is reached, a system that can steer the laser beam is used to decouple the laser from the optical cavity. The coupling of the laser to the cavity was achieved by displacing one of the mirrors with the use of a piezoelectric crystal and thus increasing and decreasing the length of the optical cavity so that resonance between the laser and the cavity can occur repeatedly[9].

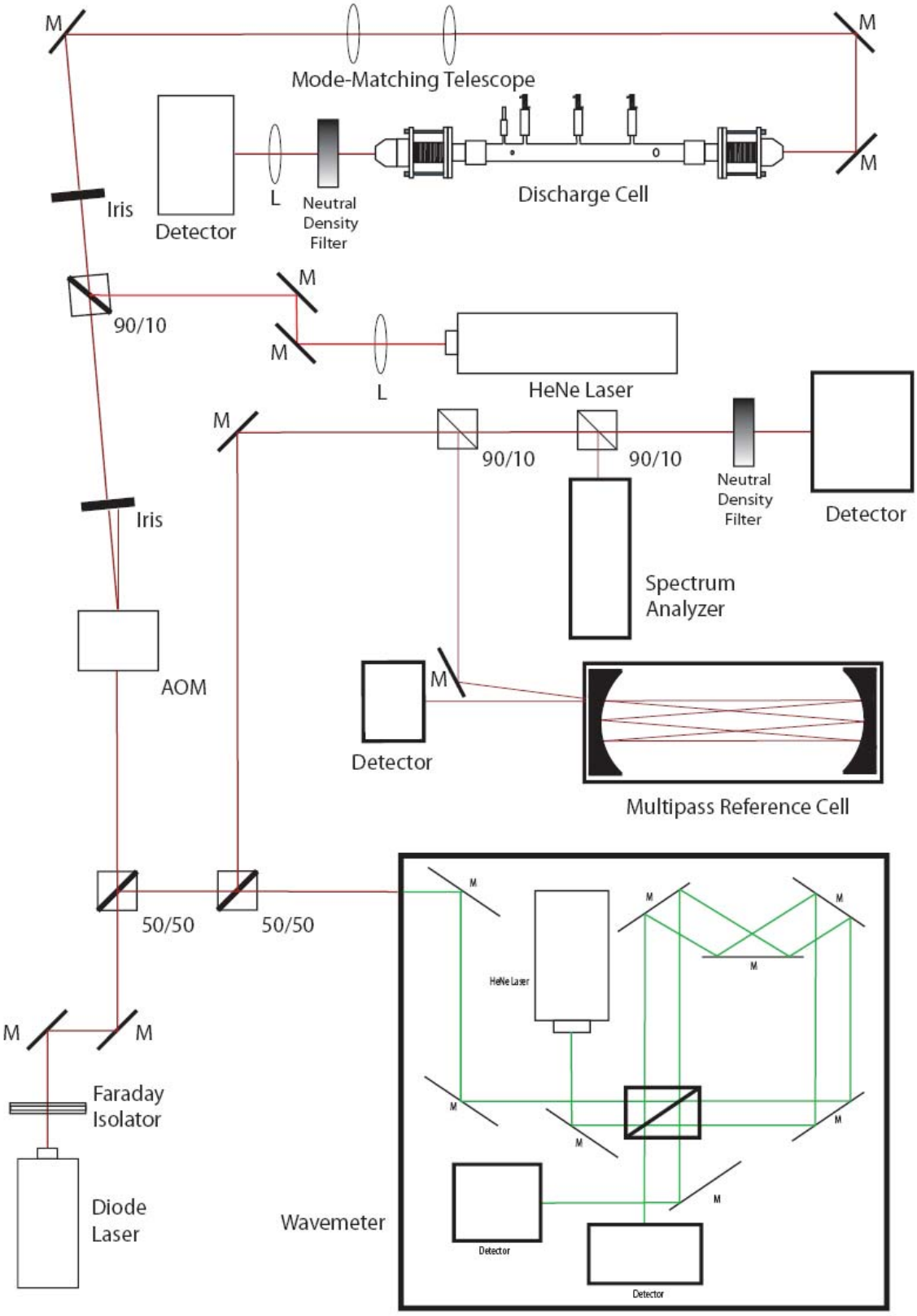

Figure 1: Continuous Wave Cavity Ringdown Spectrometer

The optical cavity is composed of two high reflectivity mirrors, R = 0.9999, in the 950nm range. These concave mirrors have a radius of curvature of 6 meters and they are placed 110 centimeters apart. One of the mirrors is attached to a piezoelectric crystal that vibrates when an oscillating voltage is applied to it. This vibration of the mirror constantly changes the cavity length, coupling the optical cavity to any frequency created by the laser, even if it is sweeping through different frequencies. This setup allows for continuous scanning over several wavenumbers and for an efficient way of acquiring spectra. Data is obtained from the cavity in the form of time decay measurements, so an optical switch is needed to deflect the laser beam away from the cavity once resonance has been achieved. This is accomplished with the use of an Acusto Optical Modulator that uses radio frequency sound waves to diffract light. The first order diffraction is coupled into the cavity since the intensity in this order can vary from 0% to about 85% of the incident beam, while the zero order diffraction is not very useful since it varies between 20% and 95% of the incident beam. The laser beam is shifted upward in frequency by 80 KHz, the radio frequency used by the AOM.

The average decay time constant obtained in this high quality optical cavity is on the order of microseconds producing an effective path length tens of kilometers long. An optical telescope was used to match the beam to the focal properties of the cavity to minimize losses and to reduce the standard deviation of the decay time by ensuring that the TEM_{00} is the only mode coupled to the cavity. This time constant is diminished greatly if losses inside the cavity are induced by an absorbing species. A small fraction of the light inside the cavity is lost with each pass, and this is detected by a detector on the opposite side of the ringdown cavity.

The infra-red diode laser used for the N_2^+ experiment was tunable over the 922 -985 nm range. The single-mode output power of the laser around the 965 nm region is over 100 milliwatts. Coarse wavelength positioning of the laser was performed by manually turning a screw that translates the grating of the laser longitudinally. A low voltage piezoelectric crystal rotated this grating whose wavelength selectivity forces the laser to oscillate in one single longitudinal mode. The scans covered 150 GHz with 1000 data points, and they were obtained by altering the voltage on the piezoelectric crystal over a range of 10 volts. Changing the voltage applied to the crystal altered the size of the crystal and thus changed the length of the optical cavity of the laser. The length of the cavity is directly correlated to the resonant wavelength of the laser, so changing the size of the cavity changed the output frequency of the laser.

The N_2^+ molecular ions were produced in a simple discharge cell, as in Figure 2. The cell was made of Pyrex glass with a diameter of ¾ of an inch and a length of 88 centimeters, and a distance of 203 millimeters between the electrodes. The cell contained three electrodes connected to glass ports perpendicular to the length of the cell with ½ inch Ultra-Torr fittings. Three more ports were included on the discharge cell. One was connected to a gauge for pressure measurements, while the other two were on the front of the cell and they were designed to be ¼ inch diameter for the gas inlet and ½ inch diameter for the gas outlet. The ends of the cell connect to a ¾ inch Ultra-Torr fitting connected to a ¾ inch stainless steel tube that is attached to a 2¾ inch conflat with a ¼ inch Swagelok connection for purge gas flow to protect the mirrors[10]. The mounts supporting the ringdown mirrors were connected to the 2¾ inch conflat with bellows that were supported by alignment screws. Two springs apply constant tension to the ringdown mounts allowing them to rest on the alignment screws.

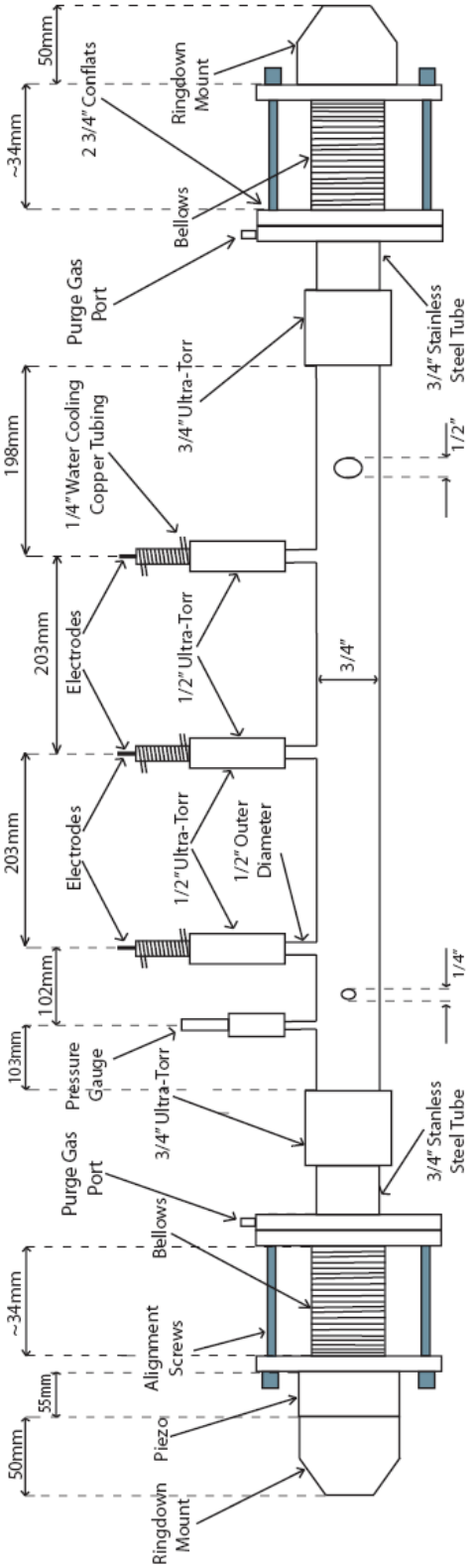

Figure 2: N_2^+ Discharge Cell

The three electrodes connected to the cell have small, stainless steel rods attached on the top side so that the power supply leads can be connected to them. Each electrode is wrapped in ¼ inch copper tubing so that cold water can be run through it for cooling. The power supply used for the discharge was a Universal Voltronics model BAL 6-300-M, which was rated for 6 kilovolts and 300 milliamps. The discharge was struck between the middle and one of the outer electrodes, while great care was taken not to produce any arcing between an electrode and the mirror mounts or the pressure sensor. To combat unwanted arcing, negative polarity was used, since the mirrors were grounded[10]. Two 10 kiloohm ballast resistors were connected in series with the middle lead, and the current of the discharge was limited to 70 milliamps, as this was found to maximize the N_2^+ signal. The voltage on the middle electrode was held at 3100 volts while the outside electrodes were grounded. The gas flown through the cell was a mixture of argon and nitrogen gas. The nitrogen was introduced in the cell through the ¼ inch inlet flange while the argon gas was the purge gas used to protect the ringdown mirrors. The ½ inch gas outlet was connected to two vacuum pumps with the help of ½ inch Teflon tubing and a ½ inch Swagelok tee-connector. The two pumps used for exhaust were a Model 1402 and a Model 1405 Duo-Seal Welch vacuum pumps[10].

The discharge cell used in this experiment was built specifically for continuous wave cavity ringdown spectroscopy. The electrodes, gas connections, and pressure probe were placed perpendicularly to the longitudinal axis of the cell so that the cavity ringdown mirrors can be placed at the ends of the cell. The relatively small size of the cell allowed for its easy placement on the optics bench. The operation of the discharge cell was simple and easily performed. The argon gas was introduced first so that a cell pressure of 300 mTorr was obtained, and nitrogen was then added so that a total pressure of 500 mTorr or 3 Torr was obtained inside the cell.

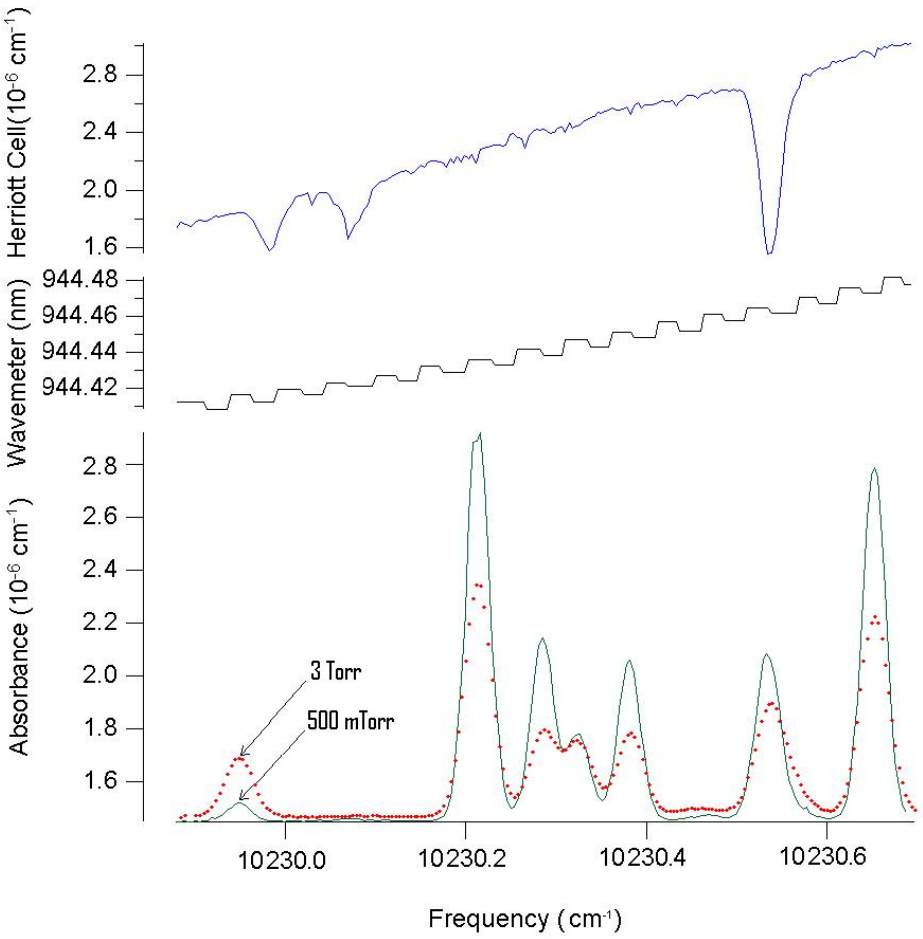

Figure 3: Sample spectrum showing the transition intensities at 3 Torr and 500 mTorr superimposed with the water spectrum obtained with the multi pass cell and the wavemeter calibration.

While performing plasma characterization for the N_2^+ discharge it was observed that the N_2^+ peak intensities varied significantly with pressure. This variation in intensity due to pressure change was a very useful feature that was used for the positive identification and assignment of the N_2^+ peaks. The N_2^+ peaks had a higher intensity at 3 Torr than they did at 500 mTorr so the spectra at the two different pressures were plotted on the same graph to allow direct comparison of peak intensities; this intensity difference is shown in Figure 3. Increased spectral complexity was observed due to the $B^3\prod_g$-$A^3\sum_u^+$ first positive group of N_2^* that was also produced in the discharge plasma. The N_2^* species was the main contaminant of the N_2^+ spectra due to the presence of nitrogen gas inside of the discharge cell and also due to the presence of multiple N_2

absorption bands in this region: (2,2), (3,3),(4,4),(5,5),(7,8), and (8,9)[12]. The line intensities of N_2^* varied with pressure as well, and fortunately this intensity fluctuation was opposite from the N_2^+ intensities. At higher nitrogen pressure the peak intensities of N_2^* were lowered due to the increased number of collisions sustained by the N_2^* molecules[13]. When considering the two spectra at the two different pressures we could easily distinguish the N_2^+ peaks from the N_2^* peaks. To aid in this analysis the two spectra were also subtracted from each other. The subtraction is shown in Figure 4, where the N_2^+ lines have positive intensities while the N_2^* lines have negative intensities.

The optics bench set up, shown in Figure 1, designed by Dr. Susanna Widicus Weaver and Brian Pohrte contains the discharge cell, a wavemeter, a Herriott cell, a tunable diode laser, a Helium-Neon laser, and various other optical elements. The incoming laser beam from the tunable diode laser was split into a reference beam and into the sample beam by a 50/50 beamsplitter. The reference beam was subsequently split by a similar beamsplitter into a beam for the interferometric wavemeter and a beam for the Herriott reference cell[10]. The sample beam was passed through the AOM at a distance of 1.353m from the laser, and the first order diffraction was selected. The sample beam was then collinearized with the beam from a 0.5 milliwatt HeNe laser introduced through a 90/10 beamsplitter to aid in alignment. The sample beam was then modematched to the ringdown cavity with an optical telescope whose center was 1.43 meters away from the AOM. The two lenses, L1 and L2 had focal lengths of 75mm and 125mm respectively, and were placed 17 cm apart. The signal detector was placed on the opposite side of the discharge cell.

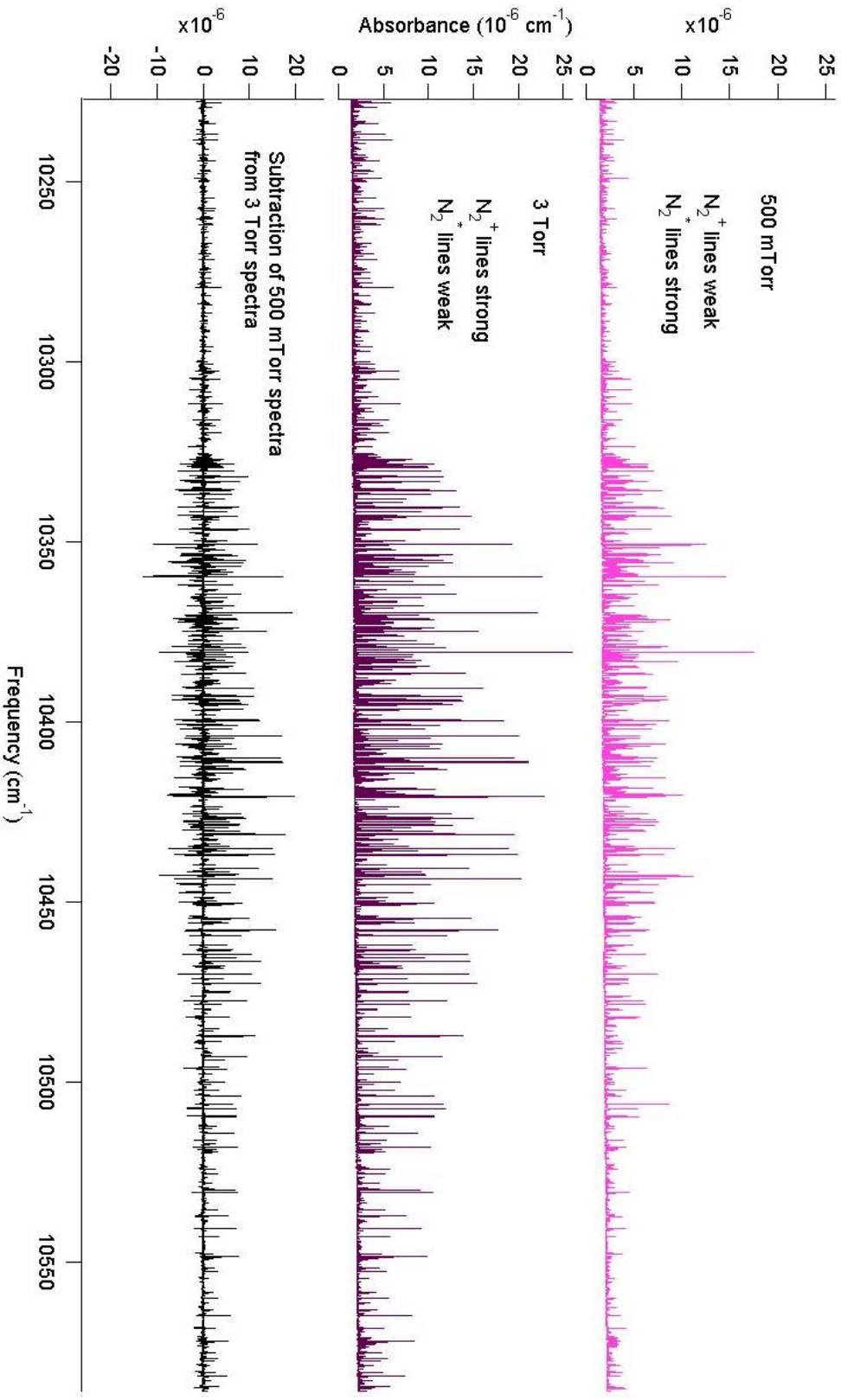

Figure 4: The complete spectra of N_2^+ at 3 Torr and 500 mTorr

The reference beam in this experiment was used for wavelength determination. The rough calibration supplied by the wavemeter was used for identifying the length of modehops that occurred during scanning. This was a traveling wavemeter based on the theory of Michelson interferometry built to work for visible/NIR lasers[10]. Michelson interferometers count the interference fringes obtained when overlapping a beam of constant length to one of varying length. The design of this wavemeter is particularly ingenious in that it has two mirrors placed on a movable cart, thus halving the distance the mirrors need to travel to collect sufficient fringes for good wavelength determination[14].

The multi pass cell was used for absolute frequency calibration and it was housed inside a 6 inch stainless steel tube that is 1 meter long and with two 8 inch flanges on each side. Two viewports were placed on the front side of the cell at a 45 degree angle so that the mirrors could be observed with ease during alignment. One of the end flanges contained four Ultra-Torr fittings with stainless steel rods running through them and supporting one of the cell mirrors, as well as a ½ inch NPT connector for gas inlet and outlet. The four rods allowed for the translation of one mirror in one axis. The opposite mirror was placed in a mount that was permanently attached to the flange. This flange contained two ¼ inch Ultra-Torr fittings with long metal turning knobs running through them, for mirror adjustment, and a one inch CaF_2 window for laser beam passage in and out of the cell. The mirrors of the cell are 3 inch gold coated mirrors. A 6 millimeter hole in the mirror attached to the flange containing the CaF_2 window allows for the entrance and exit of the laser beam. The slope of the beam exiting the Herriott cell is different than the slope entering, so the exiting beam was easily separated and redirected to a detector. After aligning the Herriott cell 20 spots were counted on each mirror, meaning that a total of 40 passes of the laser beam are obtained in the cell. Since the distance

between the mirrors was approximately 1 meter the total pathlength inside of the cell is estimated to have been about 40 meters long. The cell was filled with water vapor to a pressure of 16 mTorr. The spectrum of water in the spectral region of our laser is very well known, so comparison with the HITRAN spectra of water allowed for absolute wavelength calibration.

III. Theory:

The Meinel System of N_2^+consists of transitions between $A^2\prod_u$ and $X^2\sum_g^+$ electronic states. Shown in the energy level diagram, Figure 5, are the observed transitions in this system and the energy levels of this molecular ion. The excited state is comprised of two components, $^2\Pi_{1/2}$ and $^2\Pi_{3/2}$, and each separate energy level, for both the excited and ground level, displays a two-fold degeneracy. The A - X transitions are not perturbed by the B state or any other higher states since the v = 0 level of the B state is above the v = 9 level of the A state(4). The following section describes the energy states of N_2^+ and the prediction of the 2-1 band spectrum of this species.

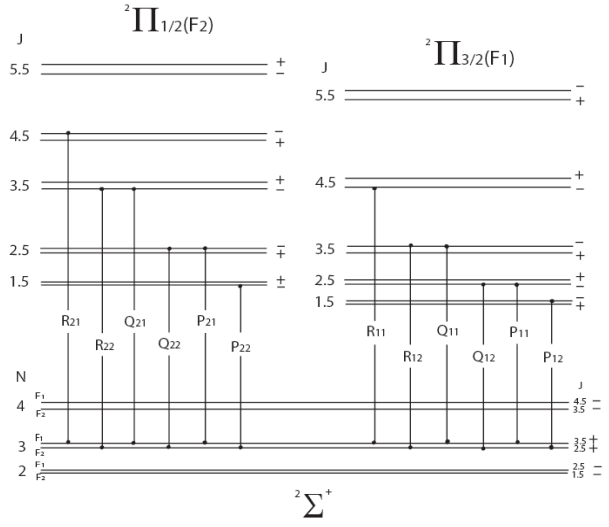

Figure 5: Energy level diagram of N_2^+

The $X^2\sum_{g^+}$ ground state conforms to Hund's case (b) allowing for a coupling between the rotational angular momentum[4], N, and the electronic spin angular momentum S. Positive spin rotation doubling is observed due to either the addition or subtraction of the electron spin resulting in the F_1 and F_2 spin components representative of the total angular momentum, J, equaling N + ½ and N – ½ respectively. The spin rotation interaction is positive because the reflection of the electronic eigenfunction across any plane going through the internuclear axis remains unchanged[15]. The Hamiltonian used for the $^2\sum$ state includes rotation, centrifugal distortion, and spin-rotation interaction and can be represented in the following way:

$$H(^2\Sigma_g^+) = B_v(r)\hat{N}^2 - D_v(r)\hat{N}^4 + \gamma(r)\hat{S}\cdot\hat{N}$$

The eigenvalues for this diagonal operator are represented by the following formulas[4]:

$$F_1(N) = B_vN(N+1) - D_v[N(N+1)]^2 + \tfrac{1}{2}\gamma N$$

$$F_2(N) = B_vN(N+1) - D_v[N(N+1)]^2 - \tfrac{1}{2}\gamma(N+1)$$

The excited electrical state however conforms to Hund's case (a), predicting twelve rotational transitions in the Meinel System[4]. The spin orbit coupling of the unpaired electron is inverted, which can be seen in the energy level diagram, Figure 5. The total angular momentum is the sum of the nuclear angular momentum R, total electronic angular momentum L, and spin angular momentum S. The S quantum number for the electron can be +½ or –½, making J equal to 3/2 or 1/2 and thus resulting in the two components of the excited state. The two fold degeneracy of the energy levels in the A state is due to Λ–type doubling, which is representative of the interaction between the rotation of the nuclei and the electronic orbital angular momentum.

$$H(^2\Pi) = B_v\hat{R}^2 - D_v\hat{R}^4 + A_v\hat{L}\cdot\hat{S} + \gamma_v\hat{S}\cdot\hat{N}$$

The standard Hamiltonian shown above was used for the upper state[6]. A 2x2 non-diagonal matrix containing the following elements was derived by Zare et al. by performing a standard Van Vleck transformation[16]:

$$\langle {}^2\Pi_{1/2},J,v,\pm \left| \mathscr{H}_{eff} \right| {}^2\Pi_{1/2},J,v,\pm\rangle = T_v^{eff} - \tfrac{1}{2}A_v^{eff} + (B_v^{eff} - D_v)(J + \tfrac{1}{2})^2 - D_v(J + \tfrac{1}{2})^4 + D_v(q_v + \tfrac{1}{2}p_v)(J + \tfrac{1}{2})$$

$$\langle {}^2\Pi_{3/2},J,v,\pm \left| \mathscr{H}_{eff} \right| {}^2\Pi_{3/2},J,v,\pm\rangle = T_v^{eff} + \tfrac{1}{2}A_v^{eff} + (B_v^{eff} + \tfrac{1}{2}A_v^{eff} + 3D_v)\ X\ [(J + \tfrac{1}{2})2 - 2] + D_v(J + 1/2)^4 - 3D_v$$

$$\langle {}^2\Pi_{1/2},J,v,\pm \left| \mathscr{H}_{eff} \right| {}^2\Pi_{3/2},J,v,\pm\rangle = T_v^{eff} - \tfrac{1}{2}A_v^{eff} + (B_v^{eff} - D_v)(J + \tfrac{1}{2})^2 - D_v(J + \tfrac{1}{2})^4 + D_v(q_v + \tfrac{1}{2}p_v)(J + \tfrac{1}{2})$$

where x = (J + ½). The parameters used in this matrix are shown and defined in Table 2. By diagonalizing this matrix the eigenvalues of the A state were obtained for each J value as well as for each positive and negative parity component.

The predicted spectrum of the 2-1 band of N_2^+ was calculated with the method used by Miller[4] and Ferguson[6]. In this technique frequencies of the spectrum are obtained by computing the appropriate differences between the eigenvalues obtained for the ground state and those obtained for the excited state. The spectra of previously observed bands have also been computed and checked with literature values to ensure the correctness of this technique. The predicted spectrum of the 2-1 rovibronic band is shown as a stick spectrum in Figure 6.

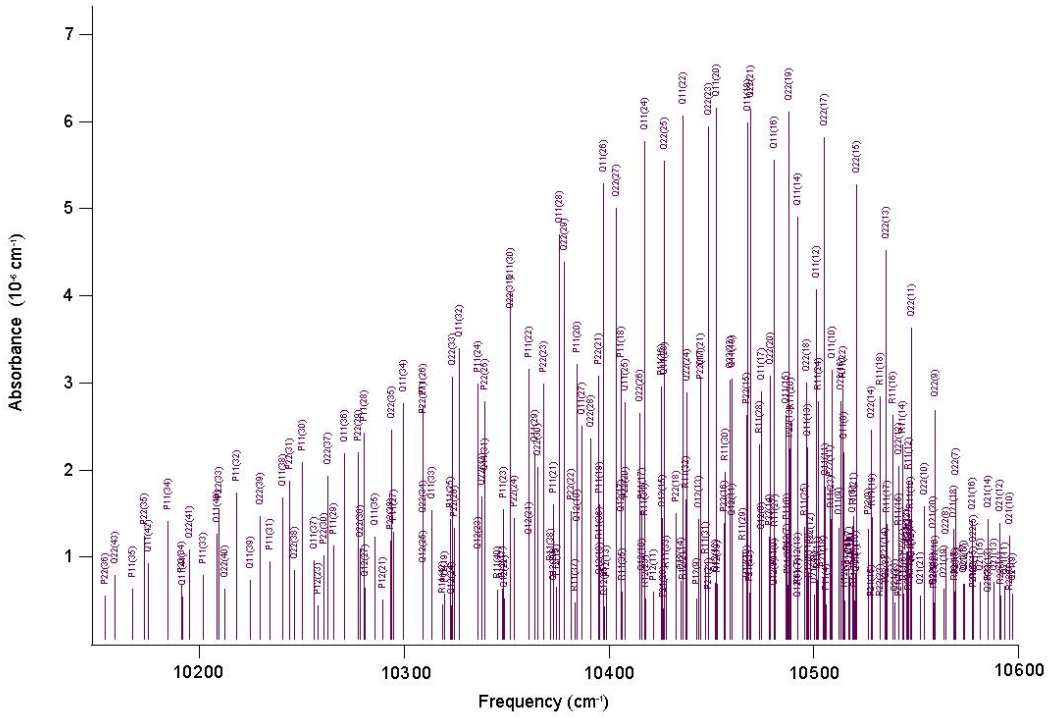

Figure 6: Predicted Spectrum of N_2^+

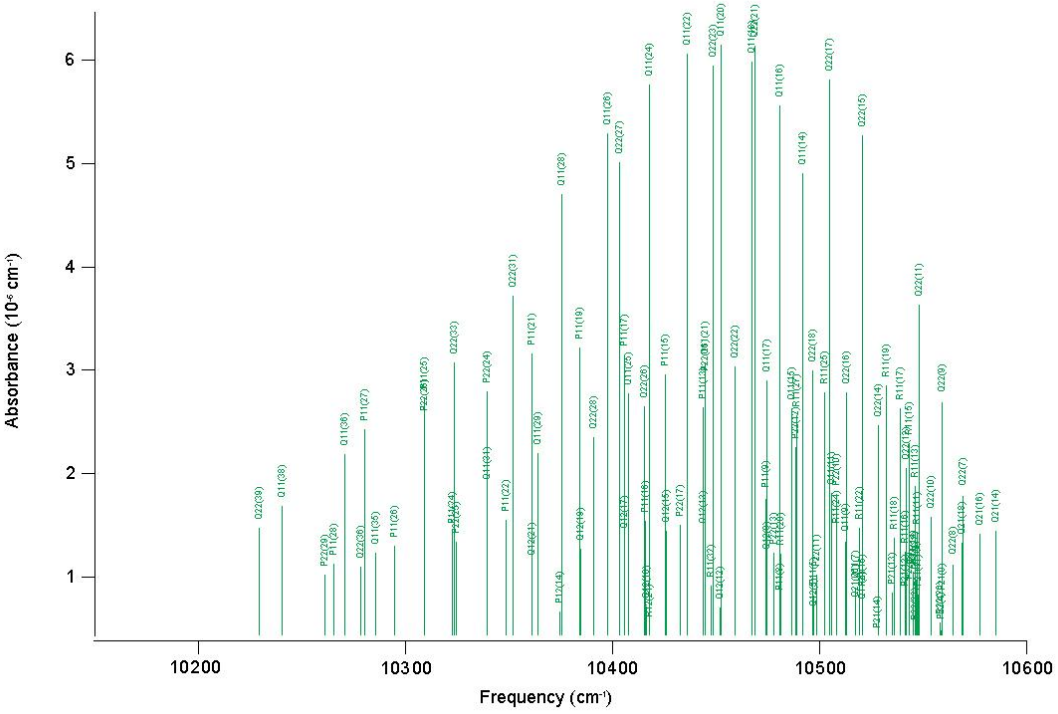

Figure 7: Assigned spectrum of N_2^+

The relative intensities of each transition shown have been calculated with the intensity formulas published by Earls[17]. If we consider U to be equal to $[\lambda^2-4\lambda + (2J+1)^2]^{-1/2}$, and λ equals the ratio between the spin orbit coupling constant and the rotational constant the transition intensity formulas are the following:

$$i_{P11} = [(2J+1)^2+U(2J+1)(4J^2+4J-7-2\lambda)]/[32(J+1)]$$

$$i_{P12} = [(2J+1)^2-U(2J+1)(4J^2+4J+1-2\lambda)]/[32(J+1)]$$

$$i_{P21} = [(2J+1)^2-U(2J+1)(4J^2+4J-7-2\lambda)]/[32(J+1)]$$

$$i_{P22} = [(2J+1)^2+U(2J+1)(4J^2+4J+1-2\lambda)]/[32(J+1)]$$

$$i_{Q11} = \{(2J+1)[(4J^2+4J-1)+U(8J^3+12J^2-2J-7-2\lambda)]\}/[32(J+1)]$$

$$i_{Q12} = \{(2J+1)[(4J^2+4J-1)-U(8J^3+12J^2-2J+1-2\lambda)]\}/[32(J+1)]$$

$$i_{Q21} = \{(2J+1)[(4J^2+4J-1)-U(8J^3+12J^2-2J-7-2\lambda)]\}/[32(J+1)]$$

$$i_{Q22} = \{(2J+1)[(4J^2+4J-1)+U(8J^3+12J^2-2J+1-2\lambda)]\}/[32(J+1)]$$

$$i_{R12} = [(2J+1)^2-U(2J+1)(4J^2+4J-7-2\lambda)]/ (32J)$$

$$i_{R11} = [(2J+1)^2+U(2J+1)(4J^2+4J+1-2\lambda)]/ (32J)$$

$$i_{R21} = [(2J+1)^2-U(2J+1)(4J^2+4J+1-2\lambda)]/ (32J)$$

$$i_{R22} = [(2J+1)^2+U(2J+1)(4J^2+4J-7-2\lambda)]/(32J)$$

If Θ is considered to be equal to $(h * v) / k_B$ and g as the spin statistical weight, then:

$$I_{PQR} = i_{PQR} * g * (2N + 1) (\Theta /T) * e^{- \Theta N(N+1)/T}$$

I_{PQR} can then be used directly for calculating the N_2^+ transitions. This prediction model allowed for the assignment of the N_2^+ lines to be possible, and it is shown in Figure 6.

IV. Results and Analysis:

The $A^2\prod_u$-$X^2\sum_{g^+}$ (2,1) band of N_2^+ was recorded in the 10200 to 10600 cm^{-1} range, where more than 550 absorption lines with an average linewidth of 0.03 cm^{-1} have been identified. Out of these lines 66 have been positively assigned to the never before observed (2,1) band using the prediction graphed in Figure 6. The observed lines are shown in Figure 7, and they are listed by branch in Table 1. The newly determined molecular parameters were used to predict the N_2^+ spectrum once more, and the difference between the observed and calculated frequencies is included in Table 1. Each absorption line was fit to a Gaussian for frequency determination. While assigning the spectrum several occasions were encountered where the N_2^+ lines were overshadowed by much larger absorption features. Since these absorption features did not vary with pressure in the same fashion as the N_2^+ lines, subtracting the spectra at differing pressures allowed us in some cases to positively identify N_2^+ absorption features.

In the process of assigning the (2,1) Meinel System band more than 450 N_2^* absorption lines have been tentatively assigned as well. Different bands from the First Positive Group of N_2^* overlap with the Meinel System (2,1) band. A significant number of N_2^+–like lines have only tentatively been assigned and were not included in the fit. The N_2^* line density was much greater than that of the corresponding molecular ion, while the absorption intensities were also significantly greater. The absorption intensities of N_2^* varied with pressure in a comparable but opposite way from those of the N_2^+ ion, so assigning the N_2^* spectrum was greatly facilitated. The lines assigned to the N_2^* species pertained to the (2,2), (3,3), (4,4), (7,8), and (8,9). A predicted spectrum was produced for all of these lines with the use of the energy levels calculated and published by Dieke and Heath[12]. These assignments are considered to be only tentative since the relative intensities of the N_2^* rovibronic transitions have not been calculated.

Table 1: The observed transitions of the (2,1) band of N_2^+ in wavenumbers (cm^{-1}).

N	P_{11}	Observed	O-C	P_{12}	Observed	O-C
5	10501.81*			10479.03*		
6	10497.24	10497.234	-0.004	10470.67*		
7	10492.2*			10461.83*		
8	10486.67`			10452.52*		
9	10480.67	10480.644	-0.023	10442.73*		
10	10474.21	10474.192	-0.006	10432.48*		
11	10467.27`			10421.76*		
12	10459.87`			10410.58*		
13	10452.01^			10398.93*		
14	10443.68	10443.683	0.013	10386.83*		
15	10434.90`			10374.28*		
16	10425.67	10425.680	0.024	10361.28*		
17	10415.99	10415.970	-0.001	10347.83*		
18	10405.85	10405.826	-0.012	10333.93*		
19	10395.28^			10319.60*		
20	10384.25"			10304.82*		
21	10372.79^			10289.60*		
22	10360.89"			10273.95*		
23	10348.55	10348.529	-0.003	10257.87*		
24	10335.78`					
25	10322.57	10322.580	0.029			
26	10308.94	10308.900	-0.013			
27	10294.87`					
28	10280.37`					
29	10265.45`					

* The transition intensity is too small

` The spectrum is missing in this region

^ N_2^+ line is overshadowed

" Tentatively assigned N_2^+ line

N	P_{21}	Observed	O-C	P_{22}	Observed	O-C
6	10577.81*			10558.82*		
7	10573.68*			10551.25*		
8	10569.21*			10543.34	10543.336	-0.009
9	10564.39*			10535.08*		
10	10559.22*			10526.47`		
11	10553.70*			10517.51*		
12	10547.81	10547.807	-0.001	10508.19	10508.192	-0.001
13	10541.57	10541.564	0.002	10498.52	10498.532	0.011
14	10534.96	10534.973	0.019	10488.50	10488.488	-0.002
15	10527.99	10527.939	-0.041	10478.11	10478.092	-0.006
16	10520.66	10520.645	0.006	10467.35`		
17	10512.95*			10456.23`		
18	10504.86^			10444.74	10444.726	-0.001
19	10496.41*			10432.88	10432.850	-0.014
20	10487.57*			10420.65^		
21	10478.36*			10408.04`		
22	10468.76*			10395.05`		
23	10458.79*			10381.69^		
24	10448.42*			10367.94`		
25	10437.67*			10353.81"		
26	10426.53*			10339.30^		
27	10415.00*			10324.40^		
28	10403.08*			10309.12"		
29	10390.77*			10293.45"		
30	10378.06*			10277.38^		
31	10364.96*			10260.93		
32	10351.47*					

* The transition intensity is too small

` The spectrum is missing in this region

^ N_2^+ line is overshadowed

" Tentatively assigned N_2^+ line

N	Q_{11}	Observed	O-C	Q_{12}	Observed	O-C
4	10520.85*			10505.94*		
5	10520.09*			10501.86*		
6	10518.85`			10497.30*		
7	10517.13^			10492.27*		
8	10514.93			10486.75*		
9	10512.27	10512.265	0.000	10480.76*		
10	10509.14`			10474.31"		
11	10505.54	10505.534	0.001	10467.38*		
12	10501.48`			10459.99`		
13	10496.95`			10452.13	10452.125	0.007
14	10491.97	10491.980	0.014	10443.82	10443.809	0.006
15	10486.54	10486.531	0.001	10435.05*		
16	10480.65	10480.644	0.003	10425.82	10425.822	0.015
17	10474.31	10474.297	-0.006	10416.15	10416.133	0.002
18	10467.53	10467.525	0.008	10406.02	10405.996	-0.011
19	10460.30`			10395.46`		
20	10452.62	10452.621	0.011	10384.44	10384.415	-0.009
21	10444.51	10444.494	-0.001	10372.99*		
22	10435.95	10435.923	-0.017	10361.10	10361.069	-0.008
23	10426.96^			10348.77*		
24	10417.53"			10336.01`		
25	10407.67	10407.661	0.004	10322.81*		
26	10397.38	10397.360	-0.002	10309.18*		
27	10386.65^			10295.12*		
28	10375.50"			10280.64*		
29	10363.92"			10265.73*		
30	10351.90^			10250.39*		
31	10339.46"					
32	10326.06^					
33	10313.31^					
34	10299.60`					
35	10285.46"					
36	10270.91"					
37	10255.93"					

* The transition intensity is too small

` The spectrum is missing in this region

^ N_2^+ line is overshadowed

" Tentatively assigned N_2^+ line

N	Q_{21}	Observed	O-C	Q_{22}	Observed	O-C
8	10598.67*			10569.29	10569.291	-0.002
9	10597.30*			10564.48	10564.502	0.022
10	10595.57"			10559.32	10559.315	-0.002
11	10593.49*			10553.80"		
12	10591.04			10547.93	10547.920	-0.002
13	10588.22*			10541.69"		
14	10585.04`			10535.10`		
15	10581.49*			10528.14	10528.129	0.006
16	10577.56"			10520.81	10520.799	0.009
17	10573.26*			10513.11	10513.104	0.016
18	10568.58	10568.561	-0.002	10505.04	10505.024	0.012
19	10563.52*			10496.59	10496.514	-0.047
20	10558.07`			10487.76`		
21	10552.24^			10478.56`		
22	10546.02	10546.001	0.010	10468.97	10468.934	-0.002
23	10539.42*			10459.00	10458.976	0.014
24	10532.42`			10448.65^		
25	10525.03*			10437.91^		
26	10517.25	10517.196	0.004	10426.78`		
27	10509.06*			10415.25"		
28	10500.49*			10403.35"		
29	10491.51*			10391.04		
30	10482.14*			10378.35`		
31	10472.36*			10365.26^		
32	10462.19*			10351.77"		
33	10451.61*			10337.89^		
34	10440.63*			10323.61"		
35	10429.24*			10308.93"		
36	10417.45*			10293.86^		
37	10405.25*			10278.38"		
38	10392.65*			10262.51^		

* The transition intensity is too small

` The spectrum is missing in this region

^ N_2^+ line is overshadowed

" Tentatively assigned N_2^+ line

N	R_{11}	Observed	O-C	R_{12}	Observed	O-C
6	10543.77*			10517.20*		
7	10524.12*			10515.01*		
8	10546.51	10546.500	-0.003	10512.36*		
9	10547.17*			10509.24*		
10	10547.36	10547.353	-0.006	10505.64*		
11	10547.09*			10501.59*		
12	10546.36	10546.361	0.007	10497.08*		
13	10545.17	10545.153	-0.005	10492.11*		
14	10543.51	10543.496	-0.008	10486.68*		
15	10541.41	10541.392	-0.004	10480.80*		
16	10538.84	10538.838	0.004	10474.47*		
17	10535.83	10535.835	0.014	10467.70*		
18	10532.37	10532.355	-0.004	10460.48*		
19	10528.47`			10452.81*		
20	10524.12"			10444.71*		
21	10519.32	10519.298	-0.002	10436.16*		
22	10514.09^			10427.18*		
23	10508.41	10508.371	-0.012	10417.76*		
24	10502.30"			10407.91*		
25	10495.75^			10397.62*		
26	10488.76"			10386.91*		
27	10481.34"			10375.76*		
28	10473.49`			10364.19*		
29	10465.20`			10352.18*		
30	10456.49`			10339.75*		
31	10447.34			10326.90*		
32	10437.76`			10313.62*		
33	10427.75*			10299.92*		
34	10417.31`			10285.79*		
35	10406.45*			10271.24*		
36	10395.16^			10256.27*		
37	10383.44*			10240.88*		

* The transition intensity is too small

` The spectrum is missing in this region

^ N_2^+ line is overshadowed

" Tentatively assigned N_2^+ line

N	R_{21}	Observed	O-C	R_{22}	Observed	O-C
8	10631.52*			10597.39*		
9	10633.59*			10595.67*		
10	10635.31*			10593.59*		
11	10636.66*			10591.15*		
12	10637.64*			10588.35*		
13	10638.25*			10585.17*		
14	10638.5*			10581.63*		
15	10638.37*			10577.72*		
16	10637.86*			10573.42*		
17	10636.97*			10568.75*		
18	10635.69*			10563.70*		
19	10634.04*			10558.26*		
20	10631.99*			10552.44*		
21	10629.56*			10546.23*		
22	10626.73*			10539.64*		
23	10623.51*			10532.65*		

* The transition intensity is too small

` The spectrum is missing in this region

^ N_2^+ line is overshadowed

" Tentatively assigned N_2^+ line

The assignment of all of the N_2^+ and N_2^* lines would not have been possible without the fitting routine constructed by Michael Wiczer. The etalon finder uses the voltage that drives the spectrum analyzer piezoelectric crystal to create a saw tooth pattern that is broken when a modehop occurs. Once a modehop is identified the wavemeter signal is used to determine the length of the modehop. Once all of the modehops and their lengths are identified the spectrum can be calibrated to relative frequency. The identification of one water line obtained from the Herriott cell is now sufficient to calibrate the whole scan. The observed water absorption lines were compared to the HITRAN[18] spectrum of water.

The analysis of the N_2^+ spectrum was performed with the fitting routine supplied by Christopher G. Tarsitano[19]. The Hamiltonians used for the rotational analysis are described in more detail in section III. The molecular parameters used to fit the data are displayed in Table 2. The value of the spin-rotation constant of the ground state was determined separately since the fit did not produce accurate results when it was included. The slope obtained from the linear graph between the R22 and Q21, Q22 and P21, R12 and Q11, Q12 and P11 combination differences and the quantum number N, shown in Figure 8, was equal to the spin-rotation constant, γ. The fitting routine was a non-linear least-squares fit performed with the Mathematica NonlinearRegress function while holding γ constant to the value previously determined. The values determined for the Hamiltonian parameters are presented in Table 2.

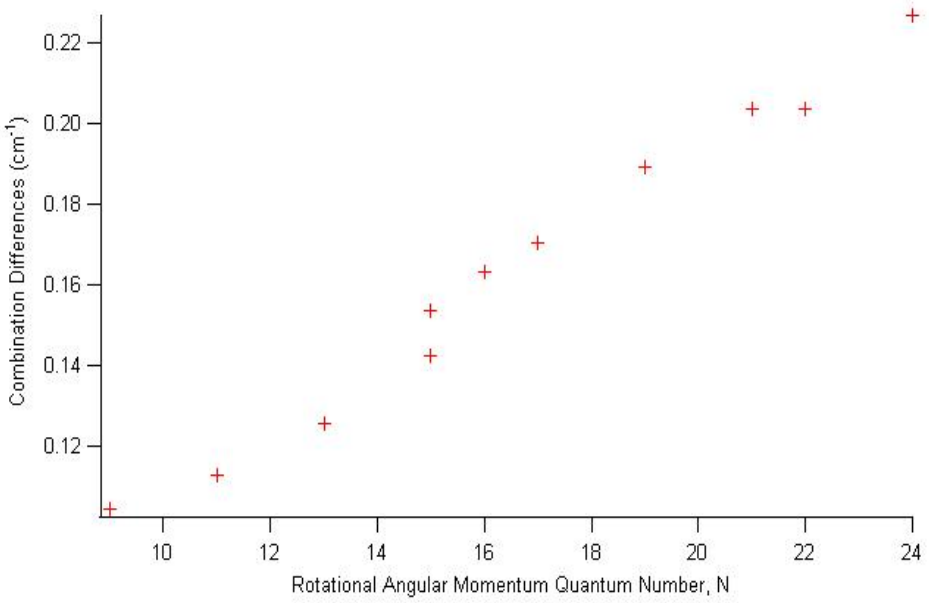

Figure 8: Spin-Rotation Constant Determination

Excited State		
T_v	vibronic term	10558.0958(62)
B_v	rotational constant	1.69756 (18)
D_v	centrifugal distortion constant	6.16 (21) 10^{-6}
A_v	spin-orbit coupling constant	-74.6509 (86)
Ad_v	effective centrifugal distortion correction to Av	-4.06 (14) 10^{-6}
q_v	lambda-doubling parameter	-0.000329 (15)
p_v	lambda-doubling parameter	0.00564(44)
	Ground State	
B_v	rotational constant for ground level	1.90365(18)
D_v	centrifugal distortion for ground level	6.24(22)10^{-6}
γ	effective spin-rotation parameter	9.31(54) 10^{-3}

Table 2: Molecular parameters in (cm^{-1}) for the (2,1) band of N_2^+

V. Conclusion:

A high resolution spectrum containing 66 assigned lines of the $A^2\prod_u$-$X^2\sum_{g^+}$ (2,1) band of N_2^+ has been obtained. The molecular parameters calculated with the least-squares fit performed have been presented in this work. Future work on this project will deal with the determination of transition intensities for the N_2^* species so that the line assignments can be verified, and a subsequent fit of the data to improve upon the N_2^* molecular constants. Once all of this work is performed an accurate determination of the plasma temperature will be possible. This continuous wave Cavity Ringdown Spectrometer will be used to study gaseous molecules of astrochemical interest in an attempt to better understand the interstellar medium.

VI. Works Cited:

1. W. H. J. Childs, Proc. R. Soc. London A 137 (1932) 641-661.
2. A. B. Meinel, Astrophys. J. 112 (1950) 562-563.
3. F. W. Dalby, and A. E. Douglas, Phys. Rev. 84 (1951) 843.
4. T. A. Miller, T. Suzuki, and E. Hirota, J. Chem. Phys. 80 (1984) 4671-4678.
5. W. Kohnlein, Earth, Moon, and Planets 47 (1989) 109-163.
6. D. W. Ferguson, K. N. Rao, P. A. Martin, and G. Guelachivili, J. Mol. Spectrosc. 153 (1992) 599-609.
7. D. Collet, J.-L. Destombes, I. Hadj Bachir, and T. R. Huet, Chem. Phys. Lett. 286 (1998) 311-316.
8. P. Dupre, and T. Gherman, J. Chem. Phys. 123 (2005) 154307.
9. D. Romanini, A. A. Kachanov, N. Sadeghi, and F. Stoeckel, Chem. Phys. Lett. 264 (1997) 316-322.
10. J. P. DiGangi, Rovibronic Spectrum of the A-X 2-1 Band of N_2^+ Utilizing Cavity Ringdown Spectroscopy (2006).
11. H. Bachir, H. Bolvin, C. Demuynck, J. L. Destombes, and A. Zellagui, J. Mol. Spectrosc. 166 (1994) 88-96.
12. G. H. Dieke, D. F. Heath, Johns Hopkins Spectroscopic Report 17 (1959).
13. B. J. McCall, and T. Oka, J. Chem. Phys. 113 (2000) 3104-3110.
14. P. J. Fox, R. E. Scholten, M. R. Walkiewicz, and R. E. Drullinger, Am. J. Phys. 67 (1999) 624-630.
15. G. Herzberg, Spectra of Diatomic Molecules. 2nd e. D. New York: Van Nostrand Company, (1950).

16. R. N. Zare, A. L. Schmeltekopf, W. J. Harrop, and D. L. Albritton, J. Mol. Spectrosc. 46 (1973) 37-66.

17. L. T. Earls, Phys. Rev. 48 (1935) 423-424.

18. The HITRAN Database, <http://www.cfa.harvard.edu/HITRAN/>, 2004.

19. C. G. Tarsitano, T. Oka, J. Mol. Spectrosc. 219 (2003) 263-270.